Brønsted Acid Sites in HSAPO-34 and Chabazite: An Ab Initio Structural Study

Yannick Jeanvoine and János G. Ángyán*

Laboratoire de Chimie Théorique, Université Henri Poincaré, UMR CNRS No. 7565, Institut Nancéien de Chimie Moléculaire, B.P. 239, 54506 Vandœuvre-lès-Nancy, France

Georg Kresse and Jürgen Hafner

Institut für Theoretische Physik, Technische Universität Wien, Wiedner Hauptstrasse 8-10, A-1040, Vienna, Austria

Received: November 26, 1997

The structure of Brønsted acid sites and the effects of the Al → Si and Si → P substitution in chabazite and $AlPO_4$-34 frameworks, respectively, have been studied by ab initio plane-wave calculations on periodic models. Geometry distortions remain well localized to the nearest neighborhood of the Brønsted acid site. The Si−O(H) and Al−O(H) distances of the common Si−O(H)−Al moiety are significantly different in the two kinds of materials. Calculated OH stretching frequencies of acidic protons, which could be assigned to the low- and high-frequency OH bands, in agreement with experimental infrared spectra of H-SSZ-13 (high silica chabazite) and HSAPO-34, correlate with OH bond lengths and Si−O(H)−Al angles.

1. Introduction

Zeolites are microporous solids with remarkable catalytic and adsorption properties, which lend them an outstanding technological importance, mainly in the field of separation and catalysis. Natural zeolites are crystalline aluminosilicates with complex framework structures, containing various arrangements of cages and channels, which can include molecules of different size in a highly specific manner. Recent progress in zeolite synthesis led to the discovery of new frameworks as well as to a considerable diversification in the composition of zeolitic materials, like Ti-, Ga-, B-, and Fe-containing zeolites and aluminophosphates.[1]

The Si/Al ratio is a crucial factor to characterize the chemical properties of zeolites. If zeolites were purely siliceous (Si/Al = ∞); i.e., if they were just modifications of silica, SiO_2, the framework would be neutral and chemically inert. Substitution of Si atoms by Al creates negative charge on the framework, compensated either by cations sitting inside the channels and cages or by protons bonded to framework oxygens and acting as Brønsted acids. Analogous Brønsted sites are formed in Si-substituted aluminophosphates (SAPOs) where some of the framework P atoms are replaced by Si. Acid sites in both types of materials play a major role in the mechanism of catalytic activity, and therefore their modeling at an atomistic level is crucial to understand their functioning.

Various theoretical approaches are available to predict geometrical parameters of zeolites and their catalytic sites. These methods have been thoroughly reviewed by Sauer[2] up to 1988 and by Sauer et al.[3] up to 1994. The simplest possible models consist of a small subset of atoms representing a fragment of the zeolite, usually terminated by H atoms. Although these cluster (or prototype molecule) models raise several problems, like that of treating properly the atoms at the boundary of the fragment or the neglect of long-range interactions as well as the effect of the zeolite cage atoms, they have the major advantage of being amenable to high-quality electronic structure calculations.[3] Long-range and/or cage effects can be partially reintroduced in cluster models by more or less sophisticated embedding techniques; see e.g. refs 4−7. In this respect, fully periodical three-dimensional models of zeolites seem to provide a more satisfactory description of zeolitic systems. Such models can be treated either by empirical potential functions[8−10] or by periodic Hartree−Fock[11] as well as density-functional calculations using plane-wave basis and pseudopotentials.[12−14] Note, however, that periodical models are not completely faithful to the physical reality in zeolites, where the distribution of substitution sites on the framework atoms usually does not follow a strictly periodical long-range order.

Precise structural features of the Brønsted acid sites are difficult to obtain experimentally since they are present only at low concentrations and appear in a disordered manner on equivalent framework sites. While neutron diffraction experiments on deuterated samples can give direct information about OH bonds, the distances and angles between protonated oxygens and their T-atom neighbors reflect only averages. Ab initio theoretical calculations provide a unique tool to obtain precise geometrical parameters of the true local structure.

The silicoaluminophosphate analogue of the aluminosilicate mineral chabazite, HSAPO-34, is an efficient catalyst with industrial applications in methanol conversion to light olefins.[15] Dehydrated H-SSZ-13, the high-silica form of chabazite, as well as HSAPO-34 have been the subject of recent structural and spectroscopic studies,[16,17] providing a detailed experimental characterization of the Brønsted acid sites in both materials.

Periodic models of these two systems have been studied recently using ab initio density functional approach by Shah, Gale, and Payne.[12,18,19] These authors characterized and compared possible acid sites in both systems.[19] On the basis of the optimized structure of zeolite−methanol complexes, they concluded that chabazite is probably more acidic than HSAPO-34.[18] Sastre et al. investigated the distribution of substitution sites in HSAPO-34 and HSAPO-5 by lattice energy calculations

* Corresponding author.

S1089-5647(98)00341-1 CCC: $15.00
Published on Web 06/29/1998

using empirical shell model,[20] attempting a geometrical and spectroscopical characterization of the bridged hydroxyls as well. In spite of the great value of these works, it seemed to be necessary to reinvestigate these systems in the light of the most recent experimental data by a powerful ab initio density-functional approach using ultrasoft pseudopotentials and plane-wave (PW) basis set. Our aim was not only to reproduce the major experimental data on these systems, but also to complete them by providing a structural and spectroscopical characterization of the Brønsted acid sites and their neighborhoods. In addition to the structure of bridged hydroxyl sites, propagation of geometrical distortions over consecutive shells of neighbors in the zeolite framework has been analyzed too. OH vibrational frequencies were calculated both in harmonic and anharmonic approximations and they were confronted with available experimental data.

In the case of hydrated HSAPO-34, experimental evidences have been reported concerning the proton (deuterium) transfer from the Brønsted acid site to adsorbed water molecules.[21] The dynamics of the proton transfer between HSAPO-34 and water, for which the better understanding of the intrinsic properties of the acid sites is of crucial importance, will be discussed in a forthcoming paper.[22]

2. Methods

Ab initio total energy calculations have been performed using the Vienna Ab initio Simulation Package (VASP).[23−26] The Kohn−Sham equations of the local-density approximation (LDA), using the exchange-correlation functional proposed by Perdew and Zunger,[27] corrected for nonlocality in the generalized gradient approximation (GGA) in the formulation of Perdew and Wang[28,29] (denoted in the following as PZPW91) have been solved variationally in a plane-wave basis set with an efficient iterative algorithm, based on the minimization of the norm of the residual vector to each eigenstate and on an effective charge-density mixing. The electron−core interactions were described by ultrasoft pseudopotentials,[30,31] which allowed us to use a relatively small cutoff of $E_c = 300$ eV. The structural results were found to be stable with respect to the increase of the plane-wave cutoff. The augmentation charges were expanded in a plane-wave basis set with a cutoff of 900 eV.

The Brillouin-zone sampling was restricted to the Γ-point. Test calculations, discussed in section 4A, using a grid of $2 \times 2 \times 2$ special k points according to the Monkhorst-Pack scheme,[32] confirmed that Γ-point calculations are sufficiently precise to obtain converged structures.

In order to avoid problems related to the incompleteness of the plane wave basis with respect to volume variations (Pulay stress[33]), complete structural relaxations were done in two steps. First, a series of relaxations was performed by optimizing the cell shape and fractional atomic coordinates at different fixed values of the volume, leading to an energy−volume, $E(V)$, curve. The relaxations were done by a quasi-Newton algorithm, using analytical forces. Structural parameters have been considered as converged when the forces on the atoms were less than 0.03 eV Å^{-1}. In a second step, the minimum of the energy−volume curve was determined by a polynomial fit and the final structural parameters were refined in a further fixed-volume relaxation at the optimal volume. In order to characterize angular deformations near the substitution and protonation sites, natural internal coordinates according to the definition of Pulay and co-workers[34] were generated by the INTCOR program[35] for subsets of atoms isolated from the periodical model.

Vibrational analysis has been limited to the OH stretching mode, which is perhaps the experimentally best understood feature in the infrared spectrum of zeolites. Calculation of the OH vibrational frequencies is facilitated by the fact that this mode can be considered as a pure one,[36] uncoupled from the rest of the motions of the zeolite structure. Harmonic OH frequencies (ω_h) were obtained as the first numerical derivatives of the analytical forces calculated at small positive and negative deformations of the OH bond. The reduced mass for the OH mode was calculated from standard atomic masses: $m_O = 15.994\,911$ and $m_H = 1.007\,830$ amu.

Anharmonic OH frequencies were obtained by a procedure described in ref 36. The OH potential energy curves have been fitted by a sixth-order polynomial in the interval from $r_0 - 0.2$ to $r_0 + 0.3$ Å around the equilibrium bond length, r_0. The lowest vibrational levels were calculated from the numerical solution of the one-dimensional nuclear Schrödinger equation using the method of ref 37 as implemented in the program ANHARM.[38] The anharmonicity constants, $\omega_e x_e$, were calculated from the two lowest transition frequencies:

$$2\omega_e x_e = 2\omega_{01} - \omega_{02} \tag{1}$$

and the corresponding harmonic frequencies were obtained from the relation

$$\omega_e = \omega_{01} + 2\omega_e x_e$$

This determination of the anharmonicity, which follows the same principles as the procedure used by experimentalists, is based on the assumption that the OH potential curve can be described by a Morse function. Although this is true to a good approximation for the OH bond, slight differences of the harmonic frequencies, ω_h and ω_e, may be observed. If the OH potential energy curves are calculated with a higher, 400 eV cutoff, the resulting frequencies are shifted by a constant value of 50−55 cm^{-1}, without changing appreciably the anharmonicites. Since the experimental difference of the OH bands associated to different protonation sites is in the order of 25−30 cm^{-1}, the frequency calculations were done with this higher cutoff.

3. Structural Models

Precise experimental determination of the structure of zeolites is quite difficult because of several obstacles. It is not common to have zeolite single crystals of sufficient size; therefore, most of the structures have been determined by powder diffraction.[39] Even if atomic positions can be found using a good initial guess of the framework structure, little is known about the occupancy of the tetrahedral (T) sites by Si, Al, or P. In fact, these atoms are almost isoelectronic and their distribution on the framework is disordered. Exceptions, like natrolite,[40] are rare. Most of the available crystal structures correspond to average framework geometries, where the nature of the T (tetrahedral) atoms cannot be specified from experimental sources. Direct observation of the Brønsted acid sites is possible by neutron diffraction experiments on deuterated samples.[16,17] However, since protons (deuterons) are distributed among symmetry-equivalent protonation sites, it is impossible to measure the amplitude of the local geometry distortions due to T-atom substitution and protonation.

The chabazite framework, common in the aluminosilicate H-SSZ-13 and silicoaluminophosphate, HSAPO-34 belongs to the trigonal system. Their structures can be described either in a hexagonal lattice, containing 48 T atoms, or in a rhombohedral one, which contains 12 T atoms per unit cell (12 Si for the siliceous model of chabazite, and 6 Al and 6 P for $AlPO_4$-34). The rhombohedral lattice, comprising a hexagonal prism of 12

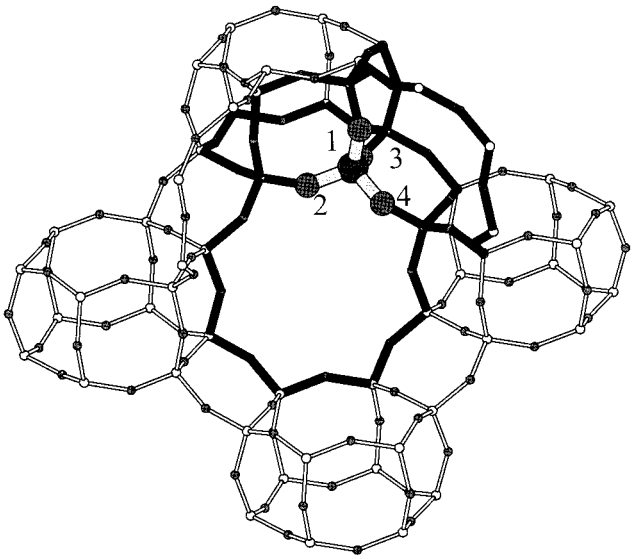

Figure 1. Framework structure of chabazite and SAPO-34 with the four distinct oxygen sites, participating in rings of different sizes. The tetrahedral sites are occupied by Si in the purely siliceous chabazite, while in $AlPO_4$-34 the P and Al cations are distributed regularly.

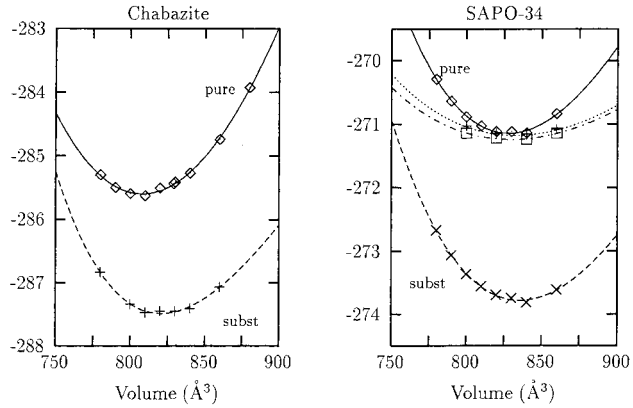

Figure 2. Total energy (eV) as a function of the unit cell volume for chabazite and SAPO-34. Full lines: energy of the ideal structure at different volumes calculated with fractional coordinates reported in Table 1. Dashed lines: energy of the O(1)-substituted model calculated at different volumes calculated with the fractional coordinates optimized at the experimental cell parameters. Dotted line: energy of the fully relaxed $AlPO_4$-34 at different volumes. In the case of $AlPO_4$-34 the potential energy curve calculated with a $2 \times 2 \times 2$ mesh of k points is displayed also (squares). In order to represent both systems on the same energy scale the curves of the ideal $AlPO_4$-34 structure have been shifted downward by 2.0 eV.

T atoms, is more appropriate for electronic structure calculations. Figure 1 shows approximately four rhombohedral unit cells (corresponding more-or-less to one hexagonal cell) to illustrate the three possible types of rings, involving 4, 6, and 8 O-atoms. In the absence of Al → Si or Si → P substitutions, all tetrahedral atoms are equivalent. The four nonequivalent oxygen sites, as represented in Figure 1, can be distinguished according to their participation in different rings of the framework. The oxygen O(1) belongs to two 4-O rings and one 8-O ring; O(2) belongs to one 4-O, one 6-O, and one 8-O ring; O(3) belongs to two 4-O and one 6-O rings; and finally O(4) participates in one 4-O and two 8-O rings.

The space group of the purely siliceous chabazite is $R\bar{3}m$, while in its aluminophosphate analogue, the alternation of Al and P atoms destroys the mirror plane, and leads to the space group $R\bar{3}$. A single Al → Si substitution in the chabazite framework, corresponding approximately to the material H-SSZ-13,[17,41] or a Si → P substitution in $AlPO_4$-34, leading to the HSAPO-34[16,21] lowers the symmetry to $P1$. Four distinct models can be constructed for both materials by a single substitution followed by the protonation of one of the nonequivalent oxygens adjacent to the substituted T atom.

4. Results and Discussion

A. Volume Relaxations. Full relaxation, involving the optimization of the atomic coordinates, of the cell shape as well as of the cell volume, has been accomplished for the $AlPO_4$-34 structure by the two-step procedure described in section 2. The minimum of the energy−volume curve (dotted line in Figure 2b) was found at 832.4 Å^3. The corresponding bulk modulus ($K_0 = 32$ GPa) has been obtained from a Burch-Murnaghan fit to the $E(V)$ curve. Extending the Brillouin-zone sampling in these calculations from the Γ point to special k points on a $2 \times 2 \times 2$ grid according to the Monkhorst-Pack scheme had a small effect on the equilibrium volume (829.6 Å^3) and the fractional coordinates as well as the cell shape changed only slightly. This demonstrates that Γ-point calculations are satisfactory for structural studies in this system.

We have attempted also to estimate the equilibrium volume by an approximate procedure, based on a energy−volume relationship resulting from single energy calculations at different volumes, while keeping the cell shape and fractional coordinates fixed.[14] Although such an approximate $E(V)$ relationship (full curves in Figure 2) cannot be considered as an equation of state, the resulting optimal volume (828.0 Å^3) agrees very well with the true equilibrium value obtained after full relaxation of all degrees of freedom. The equilibrium volume of the siliceous chabazite has been estimated by a similar approximation to be 807.9 Å^3. The same simplified procedure has been used to determine the effect of substitution on the equilibrium volumes. For both systems, a single substitution per unit cell leads to a slight increase of the volume, by about 10 Å^3 (820.8 Å^3 for chabazite, 836.0 Å^3 for HSAPO-34). This trend seems to correspond well to experimentally observed volume changes between siliceous zeolites and their substituted forms.[42]

The experimental volume of the dehydrated HSAPO-34[16] is 822.4 Å^3, while that of the hydrated sample[21] is 820.2 Å^3; both are slightly smaller than the theoretical prediction (832.4 Å^3). In the case of chabazite we can compare the theoretical estimate (807.9 Å^3) with the experimental values for the high-silica forms SSZ-13[41] (796.0 Å^3) and H-SSZ-13[17] (792.3 Å^3), both smaller than the theoretical predictions by about 10 Å^3. This behavior is probably related to a systematic error of the generalized gradient approximation (GGA), which has the tendency to overestimate equilibrium volumes, as observed in the case of silica modifications.[43]

Earlier shell model optimizations of the cell parameters of purely siliceous chabazite[12] and of $AlPO_4$-34[20] lead to smaller unit cell volumes (766.6 and 792.7 Å^3, respectively), while similar calculations on monosubstituted chabazite models[44] lead to similar (around 820 Å^3) unit cell volumes with respect to the experimental data. Fractional coordinates of the purely siliceous chabazite and of the pure aluminophosphate, $AlPO_4$-34, obtained at the experimental unit cell parameters, corresponding to volumes of 820.2 and 796.0 Å^3, are reported in Table 1. These parameters, which were held fixed during the optimization of substituted structures too, were taken from refs 21 and 41 for $AlPO_4$-34 and chabazite, respectively, and they are very close to those obtained in recent neutron diffraction measurements.[16,17]

TABLE 1: Optimized Fractional Coordinates of Siliceous Chabazite and of $AlPO_4$-34 Calculated at the Experimental Lattice Parameters[a]

	chabazite				$AlPO_4$-34		
atom	*x*	*y*	*z*	atom	*x*	*y*	*z*
Si	0.605 59	0.834 16	0.376 18	Al	0.622 40	0.166 64	0.398 08
				P	0.622 23	0.388 47	0.166 13
O(1)	0.755 67	0.244 33	0.500 00	O(1)	0.249 35	0.512 89	0.764 35
O(2)	0.651 34	0.348 66	0.000 00	O(2)	0.393 61	0.750 24	0.759 55
O(3)	0.750 60	0.750 60	0.393 77	O(3)	0.536 18	0.823 49	0.516 98
O(4)	0.523 23	0.523 23	0.830 49	O(4)	0.651 14	0.990 04	0.351 76

[a] For chabazite the space group is $R\bar{3}m$ with $a = 9.291$ Å and $\alpha = 93.92°$ and the space group is $R3$ with $a = 9.389$ Å and $\alpha = 94.33°$ for the aluminophosphate analogue. Complete lists of the optimized fractional coordinates for the four monosubstituted protonated chabazite and HSAPO-34 models are available.[54]

TABLE 2: Geometry of the Purely Siliceous Chabazite (T = Si) and the Effect of Al → Si Substitution (T = Al) on the Geometrical Parameters[a]

	exp	ideal	O(1)	O(2)	O(3)	O(4)
T−O(1)	1.617	1.616	1.904	1.691	1.692	1.700
T−O(2)	1.600	1.605	1.659	1.876	1.685	1.694
T−O(3)	1.615	1.612	1.693	1.705	1.938	1.693
T−O(4)	1.613	1.612	1.689	1.696	1.665	1.876
Si(1)−O(1)	1.617	1.616	1.702	1.580	1.577	1.581
Si(2)−O(2)	1.600	1.605	1.557	1.697	1.572	1.572
Si(3)−O(3)	1.615	1.612	1.579	1.586	1.714	1.584
Si(4)−O(4)	1.615	1.612	1.576	1.576	1.557	1.701
∠T−O(1)−Si(1)	144.7	154.1	132.9	146.1	146.2	137.9
∠T−O(2)−Si(2)	149.4	150.6	160.6	136.8	150.3	142.7
∠T−O(3)−Si(3)	147.8	150.2	151.9	142.3	135.2	145.2
∠T−O(4)−Si(4)	150.0	144.1	139.4	136.9	148.4	135.2
∠O(1)−T−O(2)	110.3	109.7	105.0	107.4	120.1	113.5
∠O(1)−T−O(3)	110.2	109.0	104.7	116.0	104.9	116.6
∠O(1)−T−O(4)	107.9	111.8	95.3	115.9	114.1	107.0
∠O(2)−T−O(3)	109.7	109.5	114.3	104.2	95.4	114.7
∠O(2)−T−O(4)	108.4	107.9	114.5	94.7	113.0	94.3
∠O(3)−T−O(4)	110.2	108.9	119.4	115.2	106.0	107.9
sym. def.(T)		−0.9	16.7	13.4	16.5	13.7
asym. def.1(T)		0.5	−0.8	−0.4	2.5	−0.5
asym. def.2(T)		−0.1	−1.9	−1.9	−0.2	−0.1
rock.1(T)		2.3	4.5	3.9	3.5	4.6
rock.2(T)		0.4	−4.9	−5.1	−5.5	4.2
sym.def. Si(1)		−0.9	9.7	−2.7	−3.8	−3.8
sym.def. Si(2)		0.6	−1.8	10.6	−0.1	−1.4
sym.def. Si(3)		1.2	−1.8	−2.3	8.8	−1.6
sym.def. Si(4)		−0.9	−0.4	−1.6	−0.6	10.9

[a] The structures are denoted by the label of the protonated oxygen. The oxygen atoms are numbered according to Figure 1, and the Si atoms are denoted corresponding to the label of the oxygen they are attached to. The experimental data are taken from the neutron diffraction study of the high-silica H-SSZ-13 material.[17]

B. Structure of Ideal and Substituted Systems. Optimized internal coordinates of the ideal and substituted chabazite and SAPO-34 materials are collected in Tables 2 and 3, where they are compared with the recent experimental data on H-SSZ-13[17] and HSAPO-34.[16] In order to compensate the systematic overestimation of equilibrium volumes by GGA, the reported calculations on the ideal siliceous chabazite and $AlPO_4$-34, as well as for the four monosubstituted H-SSZ-13 (chabazite) and HSAPO-34 models, were done at the experimental unit cell parameters. The experimental equivalence of the crystallographic axes has been maintained even in the protonated models. Optimizations including cell shape relaxation for the O(1) protonated HSAPO-34 model showed that the effect of this latter constraint is very small: the largest bond length deviations are in the order of 0.004 Å.

The Si−O bond lengths in the siliceous chabazite are between 1.605 and 1.616 Å, close to the experimentally observed range of Si−O bond lengths (1.602−1.614 Å) in simple silica phases. The P−O and Al−O distances in the $AlPO_4$-34 are between 1.526 and 1.539 Å and 1.727−1.747 Å, respectively, slightly longer than the experimental bond lengths (1.521−1.524 and 1.734−1.739 Å)[45] in berlinite, the aluminophosphate analogue of α-quartz.

TABLE 3: Geometry of the Ideal Aluminophosphate $AlPO_4$-34 (T = P) and the Effect of Si → P Substitution (T = Si) on the Geometrical Parameters[a]

	exp	ideal	O(1)	O(2)	O(3)	O(4)
T−O(1)	1.510	1.536	1.782	1.573	1.571	1.575
T−O(2)	1.548	1.526	1.556	1.760	1.565	1.571
T−O(3)	1.482	1.539	1.578	1.581	1.792	1.571
T−O(4)	1.596	1.528	1.564	1.574	1.558	1.756
Al(1)−O(1)	1.699	1.744	1.828	1.705	1.696	1.700
Al(2)−O(2)	1.666	1.727	1.682	1.817	1.686	1.687
Al(3)−O(3)	1.822	1.747	1.706	1.708	1.828	1.709
Al(4)−O(4)	1.708	1.728	1.679	1.689	1.675	1.812
∠T−O(1)−Al(1)	145.4	151.2	130.7	144.3	152.1	140.9
∠T−O(2)−Al(2)	148.3	147.8	154.6	134.1	147.6	144.3
∠T−O(3)−Al(3)	148.3	147.5	148.3	147.9	138.9	154.1
∠T−O(4)−Al(4)	152.1	145.4	151.0	142.5	148.3	134.0
∠O(1)−T−O(2)	108.8	111.1	105.6	105.1	116.7	113.0
∠O(1)−T−O(3)	111.5	110.2	103.9	113.1	104.6	114.4
∠O(1)−T−O(4)	108.2	108.6	99.7	116.1	114.9	105.5
∠O(2)−T−O(3)	109.9	108.3	113.4	106.3	98.2	117.0
∠O(2)−T−O(4)	106.9	107.7	114.3	98.1	113.7	100.4
∠O(3)−T−O(4)	111.4	111.0	117.5	115.8	106.1	104.3
sym. def.(T)		−0.9	14.5	14.5	14.9	14.0
asym. def.1(T)		−1.7	−1.4	1.4	1.9	2.7
asym. def.2(T)		1.7	−3.2	−1.9	0.9	1.0
rock.1(T)		0.5	1.0	3.81	3.80	2.6
rock.2(T)		1.9	−4.0	−4.9	−4.5	−2.8
sym.def. Al(1)		−1.7	7.3	−4.8	−6.1	−4.2
sym.def. Al(2)		1.3	−2.0	10.3	2.4	0.6
sym.def. Al(3)		−0.1	−3.0	−3.6	8.7	−3.3
sym.def. Al(4)		0.5	1.8	−0.1	0.4	10.1

[a] The structures are denoted by the label of the protonated oxygen. The oxygen atoms are numbered according to Figure 1, and the Al atoms are denoted corresponding to the label of the oxygen they are attached to. The experimental data are taken from the neutron diffraction study of the dehydrated HSAPO-34.[16]

The T−O−T′ bond angles are in the range of 144°−154° in both systems. The SiO_4, PO_4, and AlO_4 tetrahedra are only slightly distorted from the ideal shape in the unsubstituted structures, as can be judged from the O−T−O bond angles (109.5° ± 2.0°), and from the set of natural deformation coordinates, defined as appropriate linear combinations of the six O−T−O angles (cf. Figure 3).

The optimized bond lengths of the purely siliceous chabazite model are in good agreement with the experimental data for H-SSZ-13. In this system, acid sites are present in low concentration (0.7 substitutions per rhombohedral unit cell), and therefore they do not perturb appreciably the observed average framework geometry. Direct comparison is less straightforward between the optimized structure for the ideal $AlPO_4$-34 and the experimental geometry of HSAPO-34. In the latter case, acid sites occur in a higher concentration (1.32 per unit cell), and consequently the average structure measured by diffraction techniques is perturbed significantly. This is reflected by an elongation of the P−O bonds involving the proton acceptor O(2) and O(4) sites with respect to the two other P−O bonds, and also as compared to the theoretical bond lengths of the unsubstituted model. Experimental distances around the site O(3) seem to be somewhat puzzling: the P/Si−O(3) bond is even shorter than the smallest P−O distance calculated for the idealized model, while the Al−O(3) bond is almost as long as the optimized Al−O distance in the protonated model. This

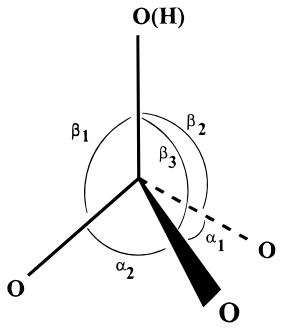

Figure 3. Natural internal coordinates describing angular deformations around a tetrahedral atom. The bond to the protonated oxygen is considered as the approximate C_3 axis of the 5-atom fragment and the five nonredundant deformation coordinates are defined by the α and β angles defined on the figure: sym.def. $= \alpha_1 + \alpha_2 + \alpha_3 - \beta_1 - \beta_2 - \beta_3$; asym.def.1 $= 2\,\alpha_1 - \alpha_2 - \alpha_3$; asym.def.2 $= \alpha_2 - \alpha_3$; rock.1 $= 2\,\beta_1 - \beta_2 - \beta_3$; rock.2 $= \beta_2 - \beta_3$.

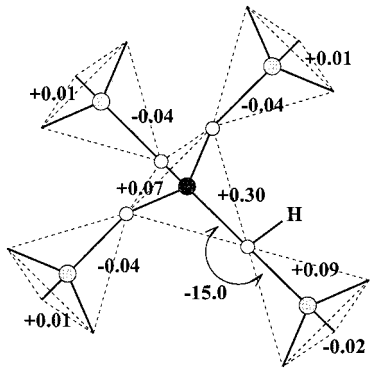

Figure 4. Approximative trends of geometry deformation in a zeolite framework due to the substitution and protonation on the geometry of the first few shells of atoms around the central substitution site, marked by dark color.

behavior can probably be attributed to the presence of strong correlations in the Rietveld refinement of the pseudo-centric HSAPO-34 structure, explaining the unusually large spread of bond distances.[46]

The calculated T−O−T′ bond angles around O(2) and O(3) agree with experiment for both systems within 2°. Theoretical predictions of 150°−155° and 145° for angles around O(1) and O(4) atoms, respectively, are in apparent contradiction with experimental values of 145° and 150° in both systems. Plane wave optimizations of Shah et al.[19] and shell-model relaxations of Sastre[20] yield O(1) and O(4) angles which are similar to the results of our calculations.

Simultaneous substitution of a tetrahedral atom and protonation on one of the adjacent oxygen sites induces distortions of the framework geometry. Although the amplitude of these distortions is somewhat smaller in HSAPO-34 than in chabazite, general trends of structural deformations are similar in both systems. The local geometrical features of the common Al−O(H)−Si moiety in chabazite and in HSAPO-34 will be discussed in more detail in section 4; here we concentrate on the trends of framework deformations summarized schematically in Figure 4.

The amplitude of the changes decreases with increasing distance from the site of the perturbation caused by substitution and protonation. One can observe the opposing phases of variations in consecutive shells of chemical bonds, which is a consequence of the bond order conservation rule, as has been pointed out by van Santen and Kramer.[47] The geometry deformations become negligible from the third shell with respect to the protonation site.

The largest deformation occurs around the substituted T atom. Substitution of Si in chabazite or P in HSAPO-34 leads to an expansion of the corresponding tetrahedron, accompanied by a deformation of its shape as a consequence of the protonation at one of the corners. The lengthening of the T−O(H) bond is considerable: 0.30 Å for chabazite and 0.25 Å for HSAPO-34. The other three T−O bonds of the central tetrahedron change much less: by 0.06−0.09 Å for chabazite and by 0.03−0.04 Å for HSAPO-34. The main contribution to the angular deformations of the central tetrahedron can be described in terms of natural coordinates defined in Figure 3 as a symmetric deformation of about 15°. The rocking and asymmetric deformation components are much smaller, practically negligible.

Among the four tetrahedra constituting the first neighbors of the substitution site, the one which shares the protonated oxygen is distorted the most significantly. This particular T′−O(H) distance increases upon protonation by 0.08−0.10 Å in both systems, while the other three T′−O bonds of the same tetrahedron shrink by 0.03 Å in chabazite and by 0.02 Å in HSAPO-34. Angular deformations are dominated by a symmetric contribution of about 10°. In the three other first-neighbor tetrahedra the T′−O distances to the oxygen shared with the central tetrahedron shrink by 0.04−0.05 Å according to the bond order conservation rule.

Among the T−O−T angles describing the bending of the corner sharing tetrahedra, the most important deformation occurs at the protonated oxygen, whose angle decreases by 10−20°, while the remaining T−O−T angles are deformed by 0−10°. The behavior of the O(4) protonation site is quite particular in this respect for both systems. The deformation is not localized to the T−O(4)−T′ angle, but it is shared with other bond angles, like T−O(1)−T′ and T−O(2)−T′, which participate in the easily deformable 8-O rings (cf. Figure 1).

Symmetric deformations of the second-shell tetrahedra are large, about +10°, in the proximity of the protonation site. There is a small but significant negative deformation up to −6° for the tetrahedra T_1 and T_3, which participate in two 4-O rings. For the other two tetrahedra T_2 and T_4, participating in two larger six- and/or eight-membered rings, the absolute value of the symmetric deformation is quite small (less than 2.5°) and it may be either positive or negative. This example demonstrates the role of topological constraints in the preferred deformation paths of the zeolite framework.

C. Relative Stability of the Protonation Sites. Both for chabazite and HSAPO-34 the calculated energy differences of the four possible proton site models, reported in Table 4, are small and remain below 2.10 kcal/mol, about twice as large as the thermal fluctuations at room temperature. The use of the generalized gradient approximation (GGA) is essential to predict meaningful energy differences. As has been shown first by Hamann[48] and confirmed by our recent calculations by VASP,[43] while the energy difference between α-quartz and stishovite is considerably underestimated in the local density approximation, the experimental value is reproduced fairly well by GGA calculations. Nevertheless, there are still approximations of the present computational approach, which may influence energy differences, although we have found that they have negligible effect on the optimized structures. Probably the most important factors would be an improved convergence of the plane wave basis as well the consideration of more *k* points. Even if one had a fully converged computational result for a given protonation site model, it should be taken into account that periodic

TABLE 4: Selected Geometrical Parameters and Relative Energies of the Optimized Structures for the Four Brønsted Site Models in H-SSZ-13 (Chabazite) and in HSAPO-34

	ΔE (kcal/mol)	O−H	Si−O	Al−O	∠Si−O−H	∠Al−O−H	∠Al−O−Si	OUT(OH)[a]
chabazite								
O(1)	0.00	0.974	1.702	1.904	116.4	110.6	132.9	0.6
O(2)	1.25	0.976	1.697	1.876	113.4	108.5	136.8	13.7
O(3)	1.43	0.975	1.714	1.938	114.8	109.1	135.2	11.6
O(4)	2.10	0.976	1.701	1.876	114.9	106.9	135.2	20.5
HSAPO-34								
O(1)	0.00	0.973	1.782	1.828	112.0	117.3	130.7	−0.2
O(2)	0.74	0.975	1.760	1.817	109.4	114.9	134.1	14.7
O(3)	2.10	0.976	1.792	1.828	107.7	113.2	138.8	6.2
O(4)	1.68	0.974	1.756	1.812	110.4	115.4	134.0	5.8

[a] OUT(OH) is the out-of-plane angle.

models differ from the real system, where acid sites are arranged on the lattice in a disordered way and entropy effects may also play a role.

In spite of these limitations, the agreement with experimental data is reasonably good. In the case of the H-SSZ-13 material, experimental data indicate that the protonation occurs on the O(1) and O(2) sites,[17] which were found to have the lowest energy in our calculations. The situation is slightly different for HSAPO-34, where the protons are believed to be located on site O(2) and O(4) in the dehydrated sample,[16] while in the hydrated sample[21] the O(1) site is coordinated by a hydroxonium ion, and the protonated O(2) site is H-bonded to a water molecule. In this case the theoretically established order of stability, O(1) < O(2) < O(4) < O(3) is only partially confirmed by the experiment: O(2) < O(4) < O(1). Two recent papers reported calculations of proton site populations in HSAPO-34. In the shell-model study of Sastre et al.[20] the relative energies for the different sites are in the range of 5 kcal/mol, the most stable being the O(2) and O(4) sites, in close agreement with experiment. The order of stability predicted by the plane wave calculations of Shah et al.[19] is similar to our results: the O(1) and O(2) sites were found the most stable both in HSAPO-34 and in chabazite.

D. Local Features of the Acid Site. The most important geometrical parameters of the protonated chabazite and HSAPO-34 models are collected in Table 4. The optimized OH bond lengths are relatively insensitive to the environment: they are between 0.973 and 0.976 Å in both systems. This is probably 0.010 Å too long, as a consequence of the systematic overestimation of the X−H bond lengths by most of the DFT functionals.[49]

The Si−O and Al−O distances are much more sensitive to the environment and vary at the different sites of the same material by about 0.03−0.06 Å. Although the Si−O(H)-Al fragment is the same in aluminosilicates and in SAPOs, the Si−O and Al−O bond lengths are quite different in these two systems. In chabazite the Si−O bond is 1.70 ± 0.01 Å and the Al−O bond is 1.91 ± 0.03 Å, while in HSAPO-34 the Si−O bond is 1.78 ± 0.02 Å and the Al−O bond is 1.82 ± 0.01 Å. According to the "average" structure of the Brønsted site, postulated by Sauer et al.[3] on the basis of various cluster models, the Si−O and the Al−O bonds would be 1.69 ± 0.03 and 1.94 ± 0.04 Å. It seems that such an "average" structural model of the acid site does not apply to SAPOs, where the Si−O bond is considerably longer and the Al−O bond is much shorter than in the aluminosilicates. The "average" model predicts correctly the Si−O bond lengths in aluminosilicates, but the Al−O distance should probably be slightly shorter in these systems.

The Al−O−Si bond angle is sensitive to the site of protonation, and it behaves analogously in the two types of materials. The proton attached to the O(1) site sits in the Al−O−Si plane both in chabazite and in HSAPO-34, reflecting the relatively symmetrical environment on the sides of the hexagonal prism. For the remaining less symmetrical sites the proton is out of the plane by 5−20°. This is less than the nonplanarity (19°−63°) found in the neutron diffraction experiments for H-SSZ-13[17] and HSAPO-34.[16] A strongly nonplanar model of the bridged hydroxyl has been recently proposed on the basis of deuterium NMR studies on different zeolites.[50] In order to check, whether we had not missed a local minimum at a higher out-of-plane angle, relaxations were done starting from strongly nonplanar Si−O(H)−Al moieties, but after a few iterations we retrieved an only slightly nonplanar geometry.

The optimal structural parameters of the acid site obtained in the present work are in reasonable agreement with previous results obtained in the literature for periodic and cluster models, using various methods like ab initio DFT, Hartree−Fock, MP2, and empirical potential calculations (Table 5). We remark that cluster model calculations yield systematically longer Al−O bond lengths, while the difference between cluster and periodic models is not very significant for the Si−O bond lengths. The plane-wave calculations of Shah et al. are distinguished by small T−O (T = Al, Si) distances, probably due to a too small lattice constant used in their optimizations. Surprisingly, in the case of their HSAPO-34 model, the Al−O and Si−O distances around the acid site are almost equal to each other,[19] the reason of which being not clear to us.

E. Vibrational Frequencies. The OH vibrational frequencies constitute one of the most efficient experimental means to characterize Brønsted acid sites and their interaction with adsorbate molecules in zeolites. They are sensitive to geometrical constraints imposed by framework atoms, as well as to the long-range electrostatic interactions in the zeolite crystal. Therefore, modeling of the system-dependent variations of OH vibrational frequencies should be based on a detailed model of the solid environment. The calculated harmonic and anharmonic as well as the experimental frequencies for the different protonation sites are summarized in Table 6.

The harmonic frequencies, ω_h, were calculated at the optimized geometries by numerical differentiation of the analytical forces. The anharmonic frequencies, ω_{01}, and the corresponding harmonic estimates, ω_e, were obtained by the approach described in section 2. The two kinds of harmonic frequencies, ω_h and ω_e, are different by about 10 cm^{-1}, indicating a slight deviation from the Morse shape of the OH potential curve. The calculated anharmonicity constants, $\omega_e x_e$, are 82.5 ± 1 cm^{-1}, in very good agreement with experimental values obtained for H-mordenite[51] and in H−ZSM-5.[52] The harmonic and anharmonic OH frequencies are underestimated by the present parametrization of the DFT theory by about 25−30 cm^{-1}. This is partly the

TABLE 5: Selected Internal Coordinates of the Acid Site Calculated for Various Models and Methods[a]

model	method	ref	O−H	Si−O	Al−O	∠Si−O−Al
offretite	CP/LDA/PW	13	0.987−0.994	1.701−1.726	1.834−1.885	139.9−161.5
chabazite	PZPW91/PW	19	0.971−0.973	1.678−1.697	1.807−1.857	132.6−134.4
chabazite	PZPW91/PW	*	0.974−0.976	1.697−1.714	1.876−1.938	132.9−136.8
HSAPO-34	PZPW91/PW	19	0.970−0.971	1.741−1.777	1.756−1.779	131.9−134.4
HSAPO-34	PZPW91/PW	*	0.973−0.976	1.756−1.792	1.812−1.828	130.7−138.8
HSAPO-34	LEM/shell	20		1.77	1.82	138.4
ZSM-18	LEM	55	0.995−1.012	1.671−1.709	1.889−1.942	131.0−155.2
faujasite	LEM/shell	10	0.954−0.969	1.689−1.696	1.894−1.947	130.2−141.8
faujasite model	HF	56	0.956	1.720	1.935	129.3
{H(AlO$_4$)}shell-1.5	HF/6-31G	57	0.952	1.704	1.985	131.8
{H(AlO$_4$)}shell-1.5	HF/6-31G*	58	0.954	1.697	1.966	
{H(AlO$_4$)}-shell-1.5	MP2/6-31G*	58	0.974	1.715	1.971	
{H(AlO$_4$)}-shell-1.5	BLYP/6-31G*	58	0.983	1.701	1.949	
{H(AlO$_4$)}shell-3	LDA	59	1.020		1.810	134.6

[a] Calculations reported in the present paper are designated by an asterisk. The cluster models are designated according to the nomenclature of Sauer.[3] {H(AlO$_4$)}shell-1.5 designates the cluster H_3Si-O-Al(OH)$_2$-OH-SiH_3.

TABLE 6: Anharmonic and Harmonic Frequencies (cm^{-1}) Calculated in H-SSZ-13 and HSAPO-34 Compared to Experimental Values[16,17] and Theoretical Estimates of Shah et al.[19]

		experiment	present work			ref 19	
		ω_{01}	ω_{01}	ω_e	ω_h	ω_{01}	ω_e
chabazite	O(1)	3603	3574	3739	3747	3590	3845
	O(2)	3579	3555	3719	3726	3565	3825
	O(3)		3557	3724	3733	3570	3830
	O(4)		3545	3710	3719	3580	3840
HSAPO-34	O(1)	3625	3590	3755	3765	3610	3870
	O(2)	3601	3572	3735	3742	3600	3860
	O(3)		3554	3718	3726	3605	3865
	O(4)	3630	3580	3745	3756	3600	3860

consequence of an overestimation of the OH bond lengths, which seems to be a common shortcoming of almost all LDA and GGA functionals with the exception of the exact-exchange B3LYP hybrid one.[53]

Absolute values of the anharmonic OH frequencies obtained by Shah et al.[19] using a third-order polynomial approximation to the Morse potential[12] are in an almost perfect agreement with experiment.[16,17] In these calculations the harmonic frequencies seem to be overestimated, compensated by an exaggeratedly strong anharmonicity of $2\omega_e x_e = 260$ cm^{-1}. In the empirical shell-model calculations for HSAPO-34,[20] absolute values of the harmonic OH frequencies are between 3750 and 3780 cm^{-1}, in the same range of values as the experimental harmonic frequencies.

Comparison between theory and experiment is more delicate for the assignment of frequencies to particular protonation sites. Shell-model calculations fail to reproduce the experimental assignment in HSAPO-34,[16,21] stating that the proton attached to sites O(1) and O(4) vibrate at a 25−30 cm^{-1} higher frequency than the proton sitting on O(2). The ab initio plane wave calculations of Shah et al. predict perfectly the splitting of 24 cm^{-1} between the O(1) and O(2) protons in chabazite, but they fail in the case of HSAPO-34, where the calculated frequencies of the O(2) and O(4) protons, experimentally split by 30 cm^{-1}, were found to be identical. Our calculations reproduce the splitting of the OH frequencies in semiquantitative agreement with experiment. In the case of H-SSZ-13 the agreement is very good, and in HSAPO-34 the O(2)/O(4) splitting is underestimated: 10 cm^{-1} vs the experimental value of 30 cm^{-1}.

Calculated frequencies display a linear regression with the OH bond lengths and the Al−O−Si angles, as illustrated in Figure 5. The data points include the four chabazite and the four SAPO-34 structures. Regression coefficients are moderately good for the full set of data points, but they are considerably improved if the points associated with the O(4) protonation sites are removed for both H-SSZ-13 and HSAPO-34. The particular behavior of the O(4) protonation site, which is manifested also in the delocalized nature of the angular deformations around this site, is probably correlated with the special conformation of the Al and Si tetrahedra in this case. While for the other bridged hydroxyls the O−T−O−H dihedral angles are 0 ± 10°, in the case of protonation at the O(4) site, the O(1)−Si−O(4)−H dihedral angle is 40°, i.e., the Si tetrahedron is in an almost staggered conformation. As a consequence, the proton on the O(4) oxygen can be coordinated by three oxygen atoms closer than 3.0 Å, while at the other

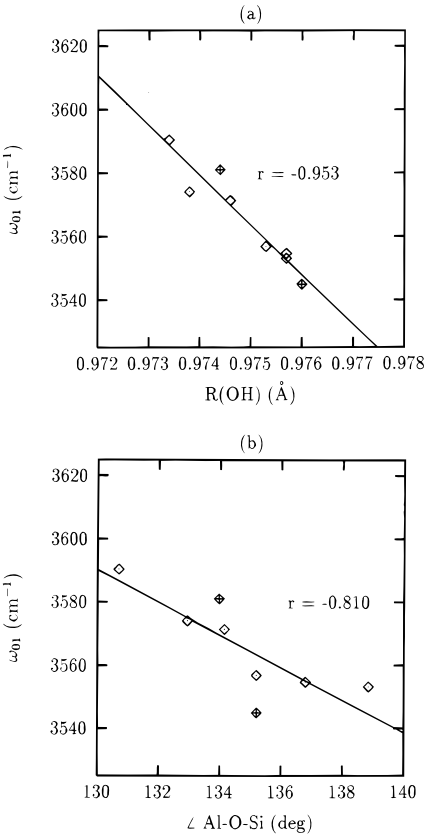

Figure 5. Correlation of the (a) OH distance and of the (b) Al−O(H)−Si angle of chabazite and HSAPO-34 with the anharmonic OH vibrational frequencies (ω_{01}). If we remove the points marked by cross, belonging to the protonated O(4) site, the correlation coefficients improve significantly: $r = -0.966$ for the OH bond length and $r = -0.940$ for the Si−O(H)−Al angle.

protonation sites only two oxygens are in the proximity of the proton. We remark that experimental neutron diffraction geometrical parameters, which reflect average instead of local geometrical features of the bridged OH groups, do not show any correlation with the measured stretching frequency.

5. Conclusions

The structures of two isotypical zeolite frameworks, the aluminosilicate chabazite and the silicoaluminophosphate SAPO-34, have been investigated by ab initio plane-wave calculations using gradient-corrected density-functional and ultrasoft pseudopotentials. The theoretically determined geometries are in reasonable agreement with experimental data and empirically established trends.

A major advantage of the ab initio calculations is that local characteristics of the bridged hydroxyls, not available by diffraction methods, can be studied too. Concerning the geometry of the Brønsted acid site, it has been found that in HSAPO-34 the Al−O bond is shorter, and the Si−O bond is longer than in the aluminosilicate chabazite. The geometry of the Al−O(H)−Si group depends also on the site of protonation, putting in evidence intrinsic limitations of the cluster models for the description of catalytic sites in zeolitic materials.

Theoretically predicted order of stability for the protonation sites in H-SSZ-13 and HSAPO-34 is in broad agreement with the experimental pieces of evidence. The calculated anharmonicity ($2\omega_e x_e = 165\ cm^{-1}$) is close to the experimental data on related systems. The difference of the calculated OH vibrational transitions corresponds to the experimentally observed splitting of the OH bands, although the absolute value of the frequencies is slightly underestimated. A good correlation has been found between OH vibrational frequencies and the local geometrical parameters of the acid site, namely the OH bond length and the Al−O(H)−Si bond angle.

Acknowledgment. This work has been accomplished in the framework of the GdR "Dynamique Moléculaire Quantique Appliquée à la Catalyse, à l'Adsorption et à l'Absorption". The financial support of the French Ministry of Education, Technology and Research is gratefully acknowledged. We thank I.D.R.I.S. (Orsay) for the generously allocated computer time. We are indebted to Professor A. K. Cheetham and Dr. L. Smith for sending us the experimental atomic coordinates of the dehydrated HSAPO-34 and a preprint of their H-SSZ-13 results prior to publication, as well as to Dr. P. Ugliengo for sending the ANHARM program.

References and Notes

(1) van Bekkum, H., Flanigen, E. M., Jansen, J. C., Eds.; *Introduction to zeolite science and practice*; Elsevier: Amsterdam, 1991.
(2) Sauer, J. *Chem. Rev.* **1989**, *89*, 199.
(3) Sauer, J.; Ugliengo, P.; Garrone, E.; Saunders: V. R. *Chem. Rev.* **1994**, *94*, 2095.
(4) Allavena, M.; Seiti, K.; Kassab, E.; Ferenczy, Gy.; Ángyán, J. G. *Chem. Phys. Lett.* **1990**, *168*, 461.
(5) Pisani, C.; Birkenheuer, U. *Int. J. Quantum Chem. Symp.* **1995**, *29*, 221.
(6) Eichler, U.; Kölmel, C. M.; Sauer, J. *J. Comput. Chem.* **1997**, *18*, 463.
(7) Greatbanks, S. P.; Hillier, I. H.; Sherwood, P. *J. Comput.Chem.* **1997**, *18*, 562.
(8) Kim, S.-C.; Keskar, N. R.; McCormick, A. V.; Chelikowsky, J. R.; Davis, H. T. *J. Chem. Phys.* **1995**, *102*, 8656.
(9) Sastre, G.; Lewis, D. W.; Catlow, C. R. A. *J. Phys. Chem.* **1996**, *100*, 6722.
(10) Schröder, K.-P.; Sauer, J. *J. Phys. Chem.* **1996**, *100*, 11043.
(11) Àpra, E.; Dovesi, R.; Freyeria-Fava, C.; Pisani, C.; Roetti, C.; Saunders: V. R. *Mod. Sim. Mater. Sci. Eng.* **1993**, *1*, 297.
(12) Shah, R.; Gale, J. D.; Payne, M. C. *J. Phys. Chem.* **1996**, *100*, 11688.
(13) Campana, L.; Selloni, A.; Weber, J.; Pasquarello, A.; Pápai, I.; Goursot, A. *Chem. Phys. Lett.* **1994**, *226*, 245.
(14) Filippone, F.; Buda, F.; Iarlori, S.; Moretti, G.; Porta, P. *J. Phys. Chem.* **1995**, *99*, 12883.
(15) Meisel, S. L.; McCullogh, J. P.; Lechthaler, C. H.; Weisz, P. B. *Chem. Technol.* **1976**, *6*, 86.
(16) Smith, L. J.; Cheetham, A. K.; Marchese, L.; Thomas, J. M.; Wright, P. A.; Chen, J.; Gianotti, E. *Catal. Lett.* **1996**, *41*, 13.
(17) Smith, L. J.; Davidson, A.; Cheetham, A. K. *Catal. Lett.* **1997**, *49*, 143.
(18) Shah, R.; Gale, J. D.; Payne, M. C. *J. Chem. Soc., Chem. Commun.* **1996**.
(19) Shah, R.; Gale, J. D.; Payne, M. C. *Phase Transitions* **1997**, *61*, 67.
(20) Sastre, G.; Lewis, D. W.; Catlow, C. R. A. *J. Phys. Chem.* **1997**, *101*, 5249.
(21) Smith, L.; Cheetham, A. K.; Morris, R. E.; Marchese, L.; Thomas, J. M.; Wright, P. A.; Chen, J. *Science* **1996**, *271*, 799.
(22) Jeanvoine, Y.; Ángyán, J. G.; Kresse, G.; Hafner, J., manuscript in preparation.
(23) Kresse, G.; Hafner, J. *Phys. Rev. B* **1993**, *48*, 13115.
(24) Kresse, G.; Hafner, J. *Phys. Rev. B* **1994**, *49*, 14251.
(25) Kresse, G.; Furthmüller, J. *Comput. Mater.Sci.* **1996**, *6*, 15.
(26) Kresse, G.; Furthmüller, J. *Phys. Rev. B* **1996**, *54*, 11169.
(27) Perdew, J. P.; Zunger, A. *Phys. Rev. B* **1981**, *23*, 8054.
(28) Perdew, J. P. In *Electronic Structure of Solids* '91/(*Berlin*, *1991*); Ziesche, P., Eschrig, H., Eds.; Akademie Verlag: Berlin, p 11.
(29) Perdew, J. P.; Burke, K.; Wang, Y. *Phys. Rev. B* **1996**, *54*, 16533.
(30) Vanderbilt, D. *Phys. Rev. B* **1990**, *41*, 7892.
(31) Kresse, G.; Hafner, J. *J. Phys. Condens. Matter* **1994**, *6*, 8245.
(32) Monkhorst, H. J.; Pack, J. D. *Phys. Rev. B* **1976**, *13*, 5188.
(33) Payne, M. C.; Teter, M. P.; Allan, D. C.; Arias, T. A.; Joannopoulos, J. D. *Rev. Mod. Phys.* **1992**, *64*, 1045.
(34) Pulay, P.; Fogarasi, G.; Pang, F.; Boggs, J. E. *J. Am. Chem. Soc.* **1979**, *101*, 2550.
(35) Fogarasi, G.; Zhou, X.; Taylor, P. W.; Pulay, P. *J. Am. Chem. Soc.* **1992**, *114*, 8191.
(36) Senchenya, I. N.; Garrone, E.; Ugliengo, P. *J. Mol. Struct. (THEOCHEM)* **1996**, *368*, 93.
(37) Lindberg, B. *J. Chem. Phys.* **1988**, *88*, 3805.
(38) ANHARM—A program to solve the monodimensional nuclear Schrödinger equation; Ugliengo, P., 1989, unpublished.
(39) Meier, W. M.; Olson, D. H. *Atlas of Zeolite Structure Types*; Butterworth: Stoneham, MA, 1992.
(40) Ghermani, N. E.; Lecomte, C.; Dusausoy, Y. *Phys. Rev. B* **1996**, *53*, 5231.
(41) Zones, S. I.; Van Nostrand, R. A. *Zeolites* **1988**, *8*, 166.
(42) Hriljac, J. A.; Eddy, M. M.; Cheetham, A. K.; Donohue, J. A.; Ray, G. J. *J. Solid State Chem.* **1993**, *106*, 66.
(43) Demuth, T.; Hafner, J.; Jeanvoine, Y.; Ángyán, J. G., manuscript in preparation.
(44) Haase, F.; Sauer, J.; Hutter, J. *Chem. Phys. Lett.* **1997**, *266*, 397.
(45) Ngo Thong; Schwarzenbach, D. *Acta Crystallogr. A* **1979**, *35*, 658.
(46) Cheetham, A. K., personal communication.
(47) van Santen, R. A.; Kramer, G. J. *Chem. Rev.* **1995**, *95*, 637.
(48) Hamann, D. R. *Phys. Rev. Lett.* **1996**, *76*, 660.
(49) Johnson, B. G.; Gill, P. M. W.; Pople, J. A. *J. Chem. Phys.* **1993**, *98*, 5612.
(50) Kobe, J. M.; Gluszak, T. J.; Dumesic, J. A.; Root, T. W. *J. Phys. Chem.* **1995**, *99*, 5485.
(51) Garrone, E.; Kazansky, V. B.; Kustov, L. M.; Sauer, J.; Senchenya, I. N.; Ugliengo, P. *J. Phys. Chem.* **1992**, *96*, 1040.
(52) Kazansky, V. B.; Kustov, L. M.; Borokov, V. Y. *Zeolites* **1982**, *3*, 77.
(53) Farnworth, K. J.; O'Malley, P. J. *J. Phys. Chem.* **1996**, *100*, 1814.
(54) Supporting information of the optimized coordinates for the chabazite and HSAPO-34 materials can be accessed from URL http://www.lctn.u-nancy.fr/supplmat/acidsites.
(55) Gale, J. D.; Cheetham, A. K. *Zeolites* **1992**, *12*, 674.
(56) Haase, F.; Sauer, J. *J. Am. Chem. Soc.* **1995**, *117*, 3780.
(57) Bates, S.; Dwyer, J. *J. Mol. Struct. (THEOCHEM)* **1994**, *306*, 57.
(58) Greatbanks, S. P.; Hillier, I. H.; Burton, N. A.; Sherwood, P. *J. Chem. Phys.* **1996**, *105*, 3770.
(59) Kyrlidis, A.; Cook, S. J.; Chakraborty, A. K.; Bell, A. T.; Theodoru, D. N. *J. Phys. Chem.* **1995**, *99*, 1505.